Received: 8 July 2020 | Revised: 3 September 2020 | Accepted: 13 October 2020

DOI: 10.1002/suco.202000416

TECHNICAL PAPER

fib CEB-FIP WILEY

Energetic damage analysis regarding the fatigue of concrete

Matthias Bode[1] | **Steffen Marx**[2]

[1]Institute of Concrete Construction, Leibniz University Hannover, Appelstraße 9a, Hannover, Germany

[2]Institute of Concrete Structures, Technische Universität Dresden, Dresden, Germany

Correspondence
Matthias Bode, Institute of Concrete Construction, Leibniz University Hannover, Appelstraße 9a, 30167 Hannover, Germany.
Email: bode@ifma.uni-hannover.de

Abstract

Due to the visco-elasto-plastic material behavior, the added energy to concrete specimens during fatigue tests is transformed into another form of energy. Besides the description of the energetic material behavior of concrete, the elastic and the plastic part of the energy as well as the dissipation energy are analyzed for different specimens. Especially the dissipation energy shows a correlation with the damage process as a result of the cyclic loading. Regarding this correlation, a new energetic damage model is introduced. With this model, a degree of damage during the tests and the development of the damage parameter over the load cycles can be determined. First tests with the developed model show good and plausible results.

KEYWORDS

dissipation energy, damage model, fatigue, warming

1 | INTRODUCTION

Despite decades of research, the damage and degradation behavior of concrete under cyclic loading has not yet been fully understood and has numerous influencing factors.[1]

Besides the analysis of the strain development and the degradation of stiffness during fatigue tests, the warming of the specimens was being on focused more in the past.[2–10] It was shown that specimens were heated up dependent on the stress amplitude, the maximum stress level and the loading frequency. Furthermore, a correlation between the increase in temperature and the damage behavior was recognized.[2]

Within this paper, the energetic behavior of concrete specimens is described first and then, pure compressive loaded fatigue tests are analyzed in an energetic manner. Thereby, a correlation between the dissipation energy and the damage process can be determined. Based on this correlation, a damage model is introduced and used for the analysis of an experimental testing series.

2 | ENERGETIC CONSIDERATION OF THE MATERIAL BEHAVIOR

Specimens or structural components dissipate energy due to their displacement as a result of the mechanical loading. This energy has to be seen as mechanical work which is physically described by the force and displacement parameters. Therefore, the stress–strain curves regarding the loading and unloading processes describe the deformation behavior as well as the energetic behavior of the material. For an ideal-elastic material behavior the loading and unloading curve are identical and according to Wischers,[11] the elastic energy E_{el} is described by the area below the curve (Figure 1).

In contrast, for an elasto-plastic material behavior, a part of the deformation is irreversible and the loading and unloading curve are shifted parallel to each other (Figure 2). While the area below the unloading curve still describes the elastic energy E_{el}, the area between the

Discussion on this paper must be submitted within two months of the print publication. The discussion will then be published in print, along with the authors' closure, if any, approximately nine months after the print publication.

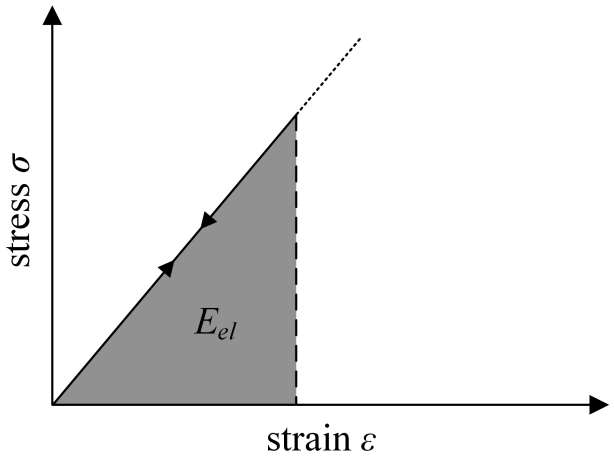

FIGURE 1 Elastic material behavior, according to *Wischers*[11]

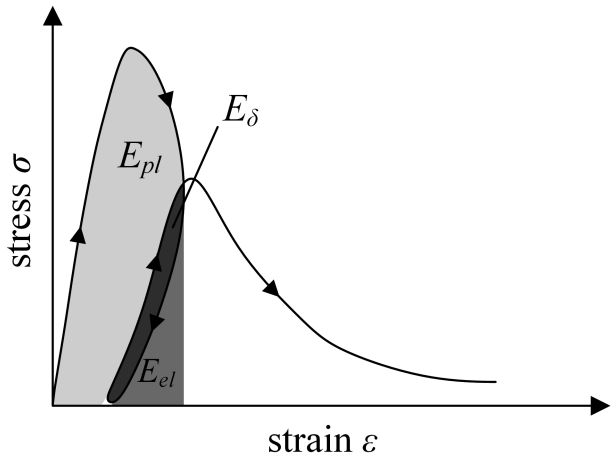

FIGURE 3 Deformation behavior of concrete, according to *Wischers*[11]

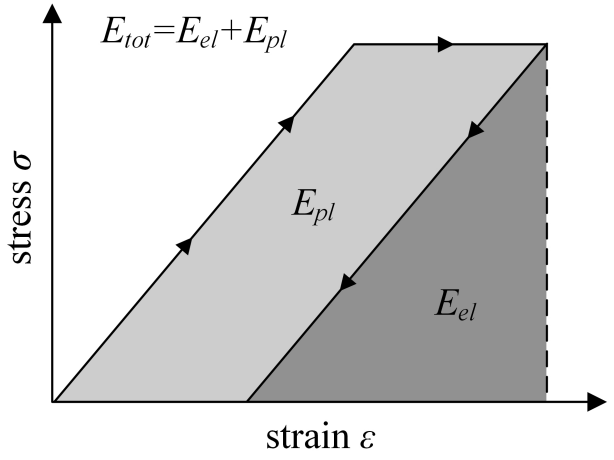

FIGURE 2 Elasto-plastic material behavior, according to *Wischers*[11]

loading and the unloading curve describes the plastic energy E_{pl}.

Besides the elastic and plastic deformation parts, the deformation behavior of concrete consists also of a viscous part. This viscous behavior is shown with the reloading curve in Figure 3. At the beginning of the reloading process, the deformation is lower than the deformation of the unloading curve before. The enclosed area is called hysteresis and characterizes the dissipation energy E_{δ}, which is described in the next chapter.

3 | DISSIPATION ENERGY

The dissipation energy E_{δ} describes the absorbed energy during a load cycle which is transformed and remains in the specimen or structural component. In the literature, this energy is sometimes also named as damping energy.[12,13] Furthermore, there are different approaches for which processes the dissipated energy is used. For Ban,[14] the cumulative dissipated energy ΣE_{δ} from all load cycles is responsible for the fatigue damage. Instead of this, Spooner et al.[15] consider only the dissipated energy E_{δ} during the first load cycles to be responsible for the damage and the dissipated energy E_{δ} during the following load cycles to be responsible for the damping behavior. Another hypothesis from Teichen[16] indicates that a major part of the dissipated energy E_{δ} is transformed into thermal energy. This hypothesis was already confirmed in a previous paper[17] and is in accordance with the observed warming of concrete specimens during fatigue tests.[2–10] Also, the explanation from Whaley[18] and Chen et al.,[19] that the friction and sliding processes between cracks and around the grains are responsible for the hysteresis and therefore for the dissipation energy E_{δ}, supports this hypothesis.

Other examinations show a significant correlation between the warming of concrete specimens and the damage behavior during fatigue tests.[2] This correlation refers to the comparison between the damage process with the warming rate at the beginning of the tests, with the temperature distribution inside and on the surface of the specimens and with the temperature development during the fatigue tests.

As a result of the temperature gradient between the specimens and their environment, a thermal energy transfer occurs. This heat loss depends on different and often unknown boundary conditions like air supply and the design of the testing machine. Therefore, as the dissipated energy describes the heat generation, which is independent of the heat loss, the direct correlation between the dissipated energy and the damage behavior is analyzed in this paper.

4 | EXPERIMENTAL STUDIES

4.1 | Testing programme

For the experimental tests, cylindrical concrete specimens with a diameter of d = 100 mm and a height of h = 300 mm were fabricated. A Portland cement CEM I 52,5 R and quarzitic aggregate with a maximum grain size of d_g = 8 mm were used. The specimens were removed from the formwork after 1 day and stored under water for additional 6 days. Afterwards, the specimens were stored in a climate chamber with standard conditions at a temperature of T_L = 20°C and a humidity of φ = 65% until they were tested. The water-cement ratio was 0.50 and the resulting 28-day compressive strength $f_{c,cyl,m,28d}$ = 64.9 MPa. After 28 days, all specimens were heated to 105°C in a drying oven for 3 days. This was done to reduce the impact of the temperature to the material properties during the fatigue tests (reduction of moisture content and avoidance of further hydration during fatigue tests). Following the 3 days in the drying oven, all specimens were stored again in the controlled climate chamber until they were tested. The used identification scheme of the specimens is only based on the chronology during their manufacturing process. Therefore, the names of the specimens do not indicate any relevant differences for the analysis of the fatigue tests.

The fatigue tests were conducted with a 2.5 MN servo-hydraulic testing machine. To adjust the stress levels, static loaded tests with a stress rate of 0.5 MPa/s were conducted immediately prior to the fatigue tests, 140 days after fabrication. Instead of a higher compressive strength compared to the 28-day compressive strength, a decrease to $f_{c,cyl,m,140d} = f_{ref}$ = 55.7 MPa was determined. Moreover, an unusual high variance regarding the six tested specimens between $f_{c,cyl,min,140d}$ = 50.5 MPa and $f_{c,cyl,max,140d}$ = 62.3 MPa occurred. It is assumed that during the warming and cooling in the drying oven some temperature induced damage processes occurred inside the specimens.

The programme for the cyclic tests consisted of 27 specimens. These specimens were tested force-controlled with a sinusoidal loading curve with loading frequencies of f_p = 2 Hz and f_p = 8 Hz. The implemented sinusoidal loading curve varied between a minimum stress level of $S_{min} = \sigma_{min} / f_{ref}$ = 0.05 and a maximum stress level $S_{max} = \sigma_{max} / f_{ref}$, according to Table 1.

Three laser distance sensors, distributed at the positions 0°, 120°, and 240° around the specimens measured the longitudinal displacement and consequently the strain of the concrete with a measuring frequency of f_m = 300 Hz (Figure 4). With the same frequency, the force was measured by a load cell. Additionally, the temperature was measured with thermocouples type T and a thermographic camera.

4.2 | Results

The S-N-curves for the tests with the loading frequencies of f_p = 2 Hz and f_p = 8 Hz are shown in Figure 5. Overall, the expected trend that higher maximum stress levels S_{max} lead to lower number of load cycles to failure N_f appears. However, the scattering of the number of load cycles to failure N_f for the different stress levels was high. This scattering can be explained by preliminary damages due to the drying procedure.[2]

By using the algorithm from Bode et al.,[20] the areas of the hysteresis for every load cycle were calculated. The algorithm was implemented in MATLAB and compares the unloading and reloading parts of the stress–strain curve to calculate the dissipation energy E_δ for every load cycle. The resulting curves of the dissipation energy E_δ per load cycle for selected specimens are shown in Figure 6 and Figure 7. For a better overview, the presented curves are already smoothed. Because of the high scattering regarding the number of load cycles to failure N_f, the analysis was done independently of the maximum stress levels S_{max}. Instead, the numbers of load cycles to failure N_f of the selected specimens are also shown in Figure 6 and Figure 7. Specimens with low numbers of load cycles to failure N_f were apparently tested on a high maximum stress level S_{max} regarding their individual compressive strength f_c and specimens with higher numbers of load cycles to failure N_f on a lower individual stress level.

It can be seen that for specimens with higher values and a stronger increase in the dissipation energy E_δ per load cycle, the failure occurs earlier than for specimens with lower values and a smaller increase. Besides, the

TABLE 1 Testing programme

Series	1	2	3	4	5	6	7	8	9
S_{max} (−)	0.80	0.80	0.75	0.75	0.70	0.70	0.65	0.65	0.60
S_{min} (−)	0.05	0.05	0.05	0.05	0.05	0.05	0.05	0.05	0.05
f_p (Hz)	8	2	8	2	8	2	8	2	8
Quantity	3	3	3	3	3	3	3	3	3

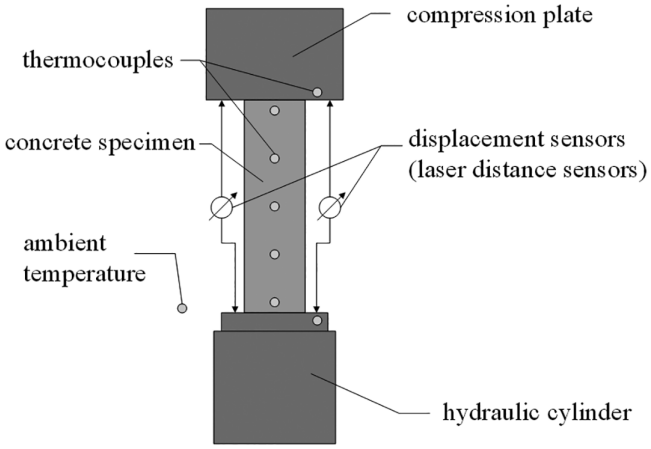

FIGURE 4 Test and measurement setup

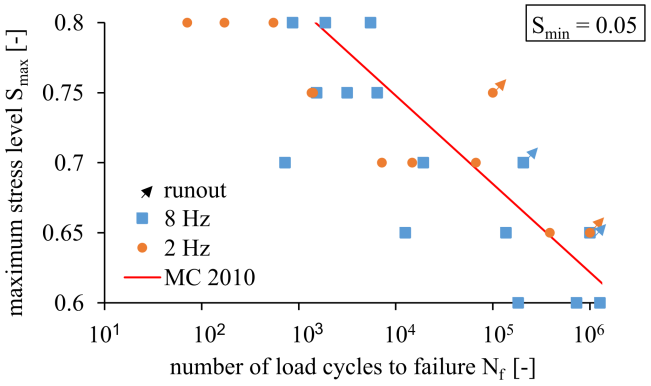

FIGURE 5 S-N curves of the experimental tests

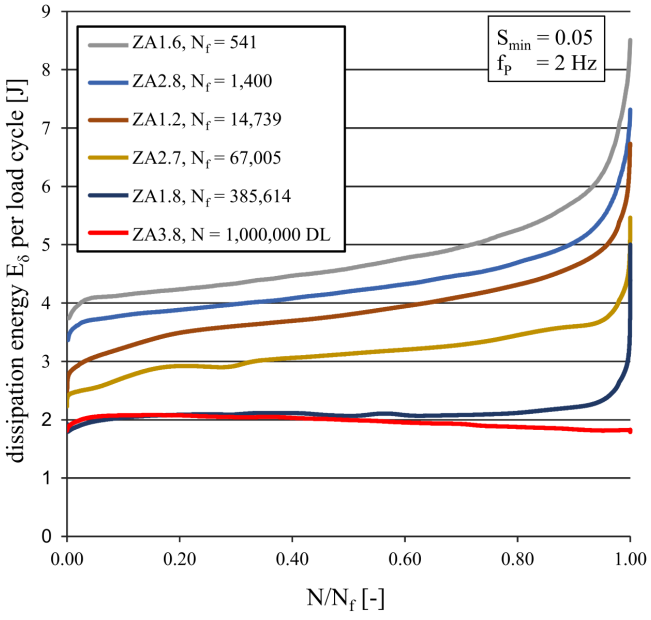

FIGURE 6 Dissipation energy E_δ per load cycle, $f_p = 2$ Hz

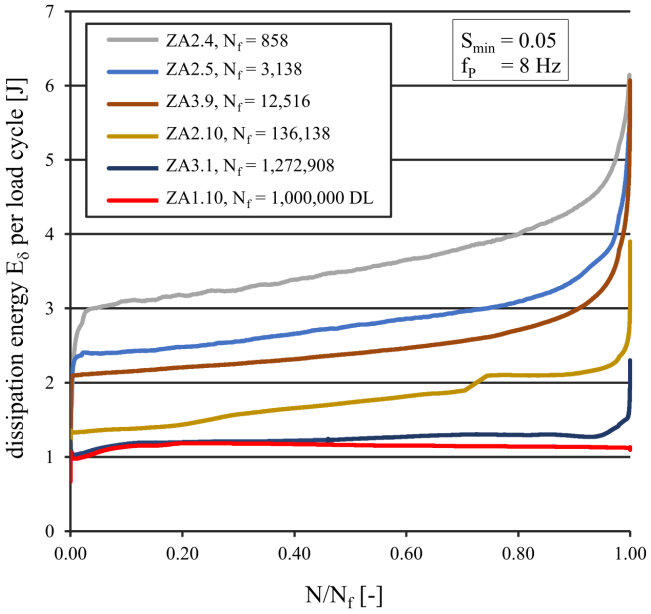

FIGURE 7 Dissipation energy E_δ per load cycle, $f_p = 8$ Hz

values from specimens with a similar number of load cycles to failure N_f are lower for specimens with a loading frequency of $f_p = 8$ Hz than for those with a loading frequency of $f_p = 2$ Hz. The typical shape with three phases, which is already known from the strain behavior and the stiffness degradation during fatigue tests, can also be seen in Figure 6 and Figure 7. After a non-linear increase in phase 1, the values develop linearly or keep constant in phase 2. Phase 3 starts shortly before failure with another non-linear increase. During the tests with the specimens ZA1.10 and ZA3.8 no failure occurred. Both tests were stopped after $N = 10^6$ load cycles. The resulting curves in Figure 6 and Figure 7 remain constant after an initial increase. Later, they are even decreasing.

A comparison of the different parts of energy for three selected specimens with significantly different number of load cycles to failure N_f in Table 2 indicates the special significance of the dissipation energy E_δ. First, the elastic energy E_{el} for the last load cycle before failure is analyzed according to Figure 1 - Figure 3. The plastic energy E_{pl} is described by the irreversible displacement. The values in Table 2 describe the plastic energy E_{pl} throughout the entire test duration. Additionally, the values for the dissipated energy E_δ per load cycle and the cumulative dissipated energy ΣE_δ until the end of the respective test were analyzed.

As the elastic energy values E_{el} seem to be smaller for specimens with a higher number of load cycles to failure N_f, this cannot be said for the plastic energy E_{pl}. Like described before, the values for the dissipated energy E_δ per load cycle are higher for specimens with a small

TABLE 2 Analysis of the different components of energy for three selected specimens

Specimen	N_f (–)	S_{max} (–)	S_{min} (–)	f_p (Hz)	E_{el} (J)	E_{pl} (J)	E_δ (J)	ΣE_δ (J)
ZA2.4	858	0.80	0.05	8	131	82	2.0–6.2	3,107
ZA3.9	12,516	0.65	0.05	8	100	95	1.2–6.1	31,203
ZA3.1	1,272,908	0.60	0.05	8	76	68	1.0–2.3	1,580,455

number of load cycles to failure N_f. Due to the higher number of load cycles, the cumulative dissipation energy ΣE_δ increases with the number of load cycles to failure N_f. The comparison of the different kinds of energy in Table 2 confirms the hypothesis from *Teichen*[16] and the results from *Vogel* et al.[17] that the dissipated energy is responsible for the warming of the specimens. Connected to the correlation between the damage behavior and the warming of the specimens,[2] in the following chapter, the straight correlation between the damage process and the dissipation energy E_δ is analyzed. Such correlation was previously analyzed by *Song* et al.,[21,22] but only for low cycle fatigue tests. A previous damage model, which was introduced by *Lei* et al.,[23] is based on constant values of the dissipation energy E_δ per load cycle and does not seem to be appropriate with the presented results in Figure 6 and Figure 7. Even if the dissipation energy is already used for a damage model and as a damage parameter[24,25] for high cycle fatigue tests, a specific analysis of the correlation is not known. Other energetic damage models, like the Envelope Concept[26,27] and the model from Pfanner,[28] are based on the elastic and plastic energy instead.

5 | ANALYSIS OF THE DISSIPATION ENERGY

To analyze a specific value of the dissipated energy E_δ per load cycle indicating an upcoming failure, the curves for the last N = 1,000 load cycles before failure for five different specimens are presented in Figure 8.

Unfortunately, the curves for the values at the end of the tests are neither identical nor parallel to each other: The lower the number of load cycles to failure N_f, the bigger the values for the dissipated energy E_δ per load cycle and the steeper the curves of the specimens. Therefore, it is not possible to indicate a critical value or a critical gradient of the dissipation energy E_δ per load cycle prognosing an upcoming failure.

Next, the cumulative dissipated energy ΣE_δ until the end of the test is analyzed. Figure 9 shows the values of the cumulative dissipation energy ΣE_δ for every specimen, tested with a loading frequency of f_p = 8 Hz, with

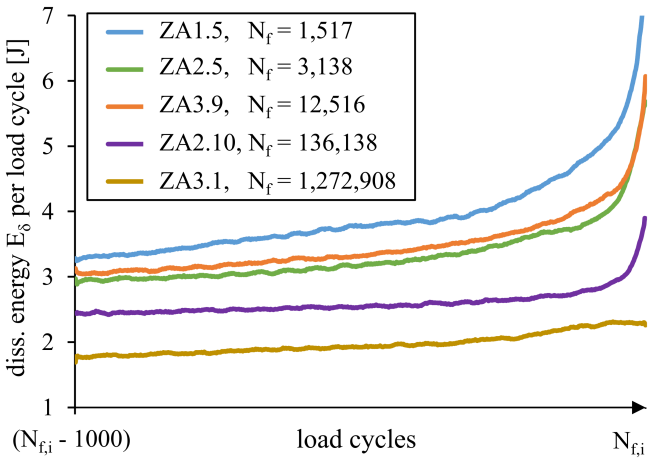

FIGURE 8 Dissipation energy E_δ per load cycle for the last 1,000 load cycles before failure, f_p = 8 Hz

regard to their number of load cycles to failure N_f. It is shown that the points from the different specimens are nearly located on a line. The corresponding curve can be described by the power function from Equation (1). The analysis of the specimens, tested with a loading frequency of f_p = 2 Hz, results in a similar functional relationship. The resulting curve can also be described by a power function which is dependent on the number of load cycles to failure N_f (Equation (2)). Both the coefficients and exponents from the two functions differ from each other.

$$\Sigma E_{\delta,fail,8Hz}(N) = 0.0107\,kJ \cdot N^{0.844}. \quad (1)$$

$$\Sigma E_{\delta,fail,2Hz}(N) = 0.0090\,kJ \cdot N^{0.897} \quad (2)$$

In this paper, the following analysis is limited to the tests with a loading frequency of f_p = 8 Hz. The obtained results for the tests with a loading frequency of f_p = 2 Hz show the same characteristics.

As shown in Figure 10, the cumulative dissipated energy ΣE_δ of a specimen is below the "line of failure" which is described by the power function from Equation (1) during the entire test. Only if the curve of a specimen's cumulative dissipation energy ΣE_δ crosses the "line of failure", does a failure occur.

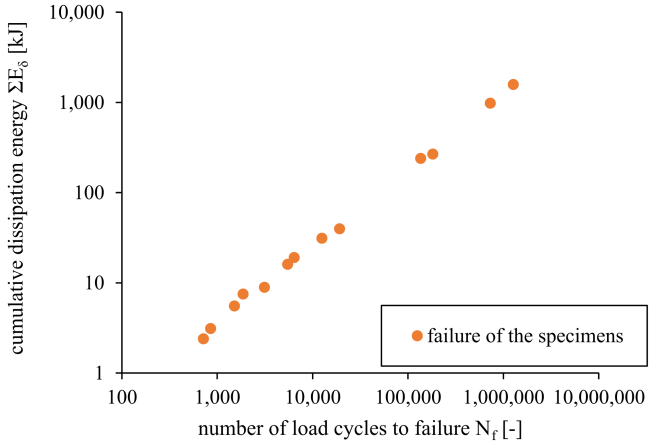

FIGURE 9 Cumulative dissipation energy ΣE_δ at the end of the test of the individual specimens, $f_p = 8$ Hz

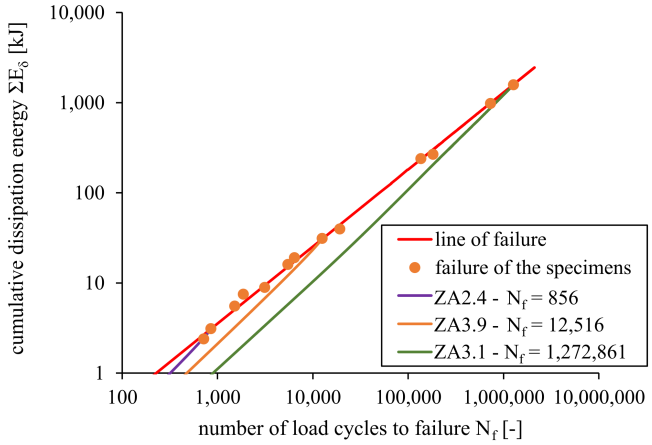

FIGURE 10 Resulting "line of failure" and the development of the cumulative dissipation energy for three selected specimens, $f_p = 8$ Hz

As the "line of failure" is described by a power function with an exponent smaller than 1.0, the gradient of the line becomes smaller for higher number of load cycles to failure N_f. Therefore, a failure occurs even for specimens with a constant progress of the dissipated energy E_δ per load cycle. This is shown by the curve of the specimen ZA3.1 in Figure 7. The values of the dissipated energy per load cycle E_δ remain constant, however, the specimen does fail. In contrast to this, the specimen ZA1.10 does not fail and the values remain nearly constant, too. This also illustrates that a conclusion cannot be drawn directly from the dissipation energy E_δ per load cycle to the damage degree of a specimen. Instead, in the following chapter the degree of damage will be analyzed by using the cumulative dissipation energy ΣE_δ.

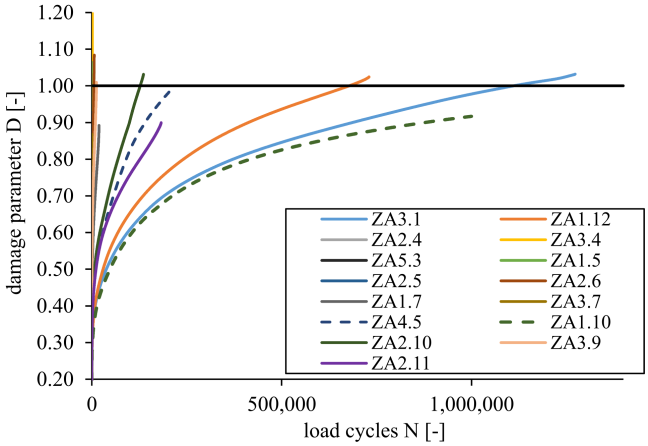

FIGURE 11 Damage parameter D(N) for different specimens, $f_p = 8$ Hz

6 | ENERGETIC DAMAGE MODEL

As described before, a failure occurs at the time when the cumulative dissipation energy $\Sigma E_{\delta,i}$ of the specimen reaches the "line of failure" (Figure 10). Based on this, a damage parameter D(N) is installed and described by Equation (3).

$$D(N) = \frac{\Sigma E_{\delta,i}(N)}{\Sigma E_{\delta,fail}(N)} \leq 1.0. \tag{3}$$

The damage parameter D(N) is characterized for every load cycle N by the ratio between the cumulative dissipation energy of a specimen $\Sigma E_{\delta,i}(N)$ and the value of the "line of failure" $\Sigma E_{\delta,fail}(N)$ of the test series. To obtain the essential "line of failure" $\Sigma E_{\delta,fail}(N)$, the values of the cumulative dissipation energy ΣE_δ and the numbers of load cycles to failure N_f from different specimens of the same test series are used. As decribed before, no more than the displacement and the force data are necessary to calculate the dissipation energy E_δ per load cycle and therefore the cumulative dissipation energy ΣE_δ. Therefore, no additional measurement devices are needed to use the introduced damage model.

In this paper, the model is used to analyze the specimens tested with a loading frequency of $f_p = 8$ Hz. The resulting curves of the damage parameter D(N) are shown in Figure 11 referring to the number of load cycles and in Figure 12 referring to the normalized test duration N/N_f. The dashed lines of the specimens ZA4.5 and ZA1.10 indicate runout tests. These tests were stopped after $N = 10^5$ load cycles (ZA4.5) or rather $N = 10^6$ load cycles (ZA1.10) without the occurrence of a failure.

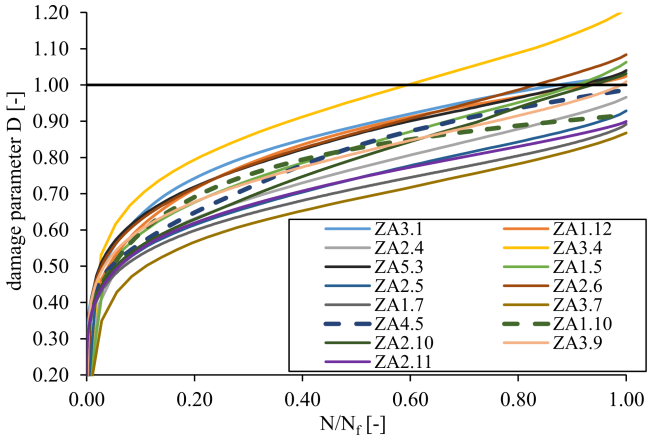

FIGURE 12 Damage parameter D(N) referring to the normalized test duration N/N_f for different specimens, $f_p = 8$ Hz

Whereas the lines in Figure 11 differ from each other, the development of the damage parameter D(N) referring to the normalized test duration N/N_f in Figure 12 is similar for the different specimens. The development of D(N) can be divided into the three phases already known from strain development and stiffness degradation for fatigue-loaded specimens. At the beginning in phase 1, the damage parameter increases rapidly. Then, the gradient decreases until the damage parameter D(N) develops nearly linearly. After a normalized test duration of $N/N_f \approx 0.80$ with the beginning of phase 3, the gradient increases until the specimen's failure. The values D(N) for the different specimens at the time of their failures are between $D(N) = 0.87$ and $D(N) = 1.21$, whereby the maximum value seems to be a single outlier. For both of the runout specimens ZA4.5 and ZA1.10 the development of the damage parameters D(N) are different and their final values are below $D(N) = 1.0$. Especially the small gradient of the specimen ZA1.10 at the end differs from the course of the other specimens and does not indicate an upcoming failure.

In contrast to the cumulative damage hypothesis of Palmgren[29] and Miner[30] that describes a linear development of the damage referring to the number of load cycles N, the curves in Figure 11 and Figure 12 describe a different damage process. The biggest difference is the strong increase at the beginning resulting in values of the damage parameter of $D(N) > 0.5$ after $N/N_f = 10\%$ of the number of load cycles to failure. In the literature, there are different research results that confirm the strong increase at the beginning. Acoustic emission results for fatigue tests from Spooner and Dougill[31] indicate that there is a large number of hits when the strain surpasses the maximum strain of the previous load cycle. Because of the known strong increase of the specimen's deformation at the beginning of a fatigue test, there is also a strong increase in the damage parameter D(N) during the first load cycles. Furthermore, the development of the damage-induced strain component from von der Haar and Marx[32] shows a similar behavior. These curves also develop in three phases with a strong increase at the beginning, followed by a linear increase during the following load cycles. Thus, the introduced damage parameter D(N) describes the damage behavior more appropriately compared to the linear development of the damage described by Palmgren[29] and Miner.[30] The varying and relative small values of the elastic and the plastic energy E_{el} and E_{pl} from Table 2 indicate the inaccuracies of the other two mentioned energetic based damage models, the Envelope Concept[26–27] and the model from Pfanner.[28] Due to the high values of the cumulative dissipation energy ΣE_δ resulting from the calculated values of the dissipation energy E_δ for every load cycle, the introduced damage model is less affected by minor measurement inaccuracies or other unintended influences.

7 | CONCLUSION AND OUTLOOK

Within this paper, on the basis of energetic analysis of fatigue-loaded concrete, a correlation between the damage process and the dissipation energy is shown. The developed damage model can be used for the valuation of the degree of damage during the testing as well as for the analysis of the damage progress referring to the entire test duration and the evaluation of the runout specimens. Especially the small scattering and the different development of the damage parameter D(N) of the runout specimen ZA1.10 indicate the suitability of the model. Furthermore, the comparison with the acoustic emission tests from Spooner and Dougill[31] and the damage-induced strain component from von der Haar and Marx[32] verify the model.

Because of the dependence of the damage parameter D(N) on the specific "line of failure", the line's function needs to be determined for every testing series. Further research showed that the functions are dependent on the loading frequency f_p, the minimum stress level S_{min} and the individual concrete type. The exact impact from the different parameters needs to be examined in more detail. Besides, the model which is limited to fatigue tests with constant stress levels S_{min} and S_{max} so far, is being extended for multi-level fatigue tests. The first analysis indicates good results which will be published in the near future.

ACKNOWLEDGMENTS

The authors would like to thank the Deutsche Forschungsgesellschaft (DFG) for their financial support

of the research project "Causes and modeling of the warming of fatigue-loaded concrete specimens" (MA5296/8-1).

DATA AVAILABILITY STATEMENT

The data that support the findings of this study are available from the corresponding author upon reasonable request.

ORCID

Matthias Bode https://orcid.org/0000-0002-0136-9083

REFERENCES

1. Marx S, Grünberg J, Hansen M, Schneider S. Sachstandbericht Grenzzustände der Ermüdung von dynamisch hoch beanspruchten Tragwerken aus Beton. Deutscher Ausschuss für Stahlbeton. 2017;Heft 618.
2. Bode M, Marx S. Heat generation during fatigue tests on concrete specimens. Concrete - innovations in materials, design and structures. Proc fib Symp. 2019;47:1881–1887.
3. Elsmeier K. Influence of temperature on the fatigue behavior of concrete. Concrete - Innovation and Design. Proc fib Symp. 2015;No. 41.
4. von der Haar C, Wedel F, Marx S. Numerical and experimental investigations of the warming of fatigue-loaded concrete. Performance-based approaches for concrete structures. Proc fib Symp. 2016;No. 42.
5. Hümme J, von der Haar C, Lohaus L, Marx S. Fatigue behaviour of a normal-strength concrete – number of cycles to failure and strain development. Struc Concrete. 2016;17(4):637–645. https://doi.org/10.1002/suco.201500139.
6. Elsmeier K, Lohaus L. Temperature development of concrete due to fatigue loading. Proc fib Phd Symp. 2014;No. 40: 137–142.
7. Otto C, Elsmeier K, Lohaus L. Temperature effects on the fatigue resistance of high-strength-concrete and high-strength-grout. High tech concrete: Where technology and engineering meet. Proc fib Symp. 2017;1401–1409. https://doi.org/10.1007/978-3-319-59471-2_161.
8. Deutscher M, Tran NL, Scheerer S. Experimental investigations on the temperature increase of ultra-high performance concrete under fatigue loading. Appl Sci. 2019;9:4087.
9. Markert M, Birtel V, Garrecht H. Temperature and humidity induced damage processes in concrete due to pure compressive fatigue loading. Concrete - Innovations Mater Design Struc. Proc fib Symp. 2019;47:1928–1935.
10. Schneider S, Hümme J, Marx S, Lohaus L. Untersuchungen zum Einfluss der Probekörpergröße auf den Ermüdungswiderstand von hochfestem Beton. Beton- und Stahlbetonbau. 2018;113(1): 58–67. https://doi.org/10.1002/best.201700051.
11. Wischers G. Aufnahme und Auswirkungen von Druckbeanspruchungen auf Beton. Betontechnische Berichte, Forschungsinstitut der Zementindustrie. 1978;(2/78):63–67.
12. Jordan RW. The effect of stress, frequency, curing, mix and age upon the damping of concrete. Magazine of Concrete Research. 1980;32(113):195–205.
13. Cole DG, Spooner DC. The damping capacity of concrete. Proc Int conf. 1968;217–225.
14. Ban S. Der Ermüdungsvorgang von Beton. Der Bauingenieur. 1933;Heft 13/14:188–192.
15. Spooner DC, Pomeroy CD, Dougill JW. Damage and energy dissipation in cement pasts in compression. Magazine Concrete Res. 1976;28:21–29.
16. Teichen, K.-T. Über die innere Dämpfung von Beton. [Phd Thesis]. Stuttgart, Germany, 1968.
17. Vogel A, Völker C, Bode M, Marx S. Messung und Simulation der Erwärmung von ermüdungsbeanspruchten Betonprobekörpern. Bauphysik. 2020;42(2):86–93. https://doi.org/10.1002/bapi.201900031.
18. Whaley, C. P. The creep of concrete under cyclic uniaxial compression. [Phd thesis]. Leeds, UK, 1971
19. Chen X, Huang Y, Chen C, Lu J, Fan X. Experimental study and analytical modeling on hysteresis behavior of plain concrete in uniaxial cyclic tension. Int J Fatigue. 2017;96:261–269. https://doi.org/10.1016/j.ijfatiugue.201612002.
20. Bode M, Marx S, Vogel A, Völker C. Dissipationsenergie bei Ermüdungsversuchen an Betonprobekörern. Beton- und Stahlbetonbau. 2019;114(8):548–556. https://doi.org/10.1002/best.201900004.
21. Song Z, Frühwirt T, Konietzky H. Characteristics of dissipated energy of concrete subjected to cyclic loading. Construction Building Mater. 2018;168:47–60. https://doi.org/10.1016/j.conbuildmat.201802076.
22. Song Z, Konietzky H, Frühwirt T. Hysteresis energy-based failure indicators for concrete and brittle rocks under condition of fatigue loading. Int J Fatigue. 2018;114:298–310. https://doi.org/10.1016/j.ijfatiugue.201806001.
23. Lei Z, Pei Z, Pengxiang B, Feipeng Z. Fatigue life prediction method of concrete based on energy dissipation. Construction Building Mater. 2017;145:419–425. https://doi.org/10.1016/j.conbuildmat.201704030.
24. Otto C, Oneschkow N, Lohaus L. Difference between the fatigue behaviour of high-strength grout and high-strength concrete. Concrete - innovations in materials, design and structures. Proc fib Symp. 2019;47:1936–1943.
25. Scheiden T, Oneschkow N. Influence of coarse aggregate type on the damage mechanism in high-strength concrete und compressive fatigue loading. Struc Concrete. 2019;20(4):1212–1219. https://doi.org/10.1002/suco.201900029.
26. Sinha BP, Gerstle KH, Tulin LG. Stress-strain relations for concrete under cyclic loading. J American Concrete Institute. 1964;(2):195–211.
27. Karsan ID, Jirsa JO. Behavior of concrete under compressive loadings. J Struc Division (ASCE). 1969;95(12):2543–2563.
28. Pfanner, D. Zur Degradation von Stahlbetonbauteilen unter Ermüdungsbeanspruchung. [Phd Thesis]. Bochum, Germany, 2003.
29. Palmgren A. Die Lebensdauer von Kugellagern. Zeitschrift des Vereins deutscher Ingenieure, 1924. 68:339–341.
30. Miner MA. Cumulative damage in fatigue. J Appl Mech. 1945; 12: A159–A164.
31. Spooner DC, Dougill JW. A quantitative assessment of damage sustained in concrete during compressive loading. Magazine Concrete Res. 1975;27:151–160.
32. von der Haar C, Marx S. A strain model for fatigue-loaded concrete. Struc Concrete. 2018;19(2):463–471. https://doi.org/10.1002/suco.201700029.

AUTHOR BIOGRAPHIES

Matthias Bode, Institute of Concrete Construction, Leibniz University Hannover, Appelstraße 9a, 30167 Hannover, Germany.

Steffen Marx, Institute of Concrete Structures, Technische Universität Dresden, 01062 Dresden, Germany.

How to cite this article: Bode M, Marx S. Energetic damage analysis regarding the fatigue of concrete. *Structural Concrete*. 2021;22(Suppl. 1): E851–E859. https://doi.org/10.1002/suco.202000416